

Article

# Forced Convection of Fe<sub>3</sub>O<sub>4</sub>-Water Nanofluid in a Bifurcating Channel under the Effect of Variable Magnetic Field

Fatih Selimefendigil <sup>1,\*</sup>, Hakan F. Oztop <sup>2,3</sup>, Mikhail A. Sheremet <sup>4,\*</sup> and Nidal Abu-Hamdeh <sup>3</sup><sup>1</sup> Department of Mechanical Engineering, Celal Bayar University, Manisa 45140, Turkey<sup>2</sup> Department of Mechanical Engineering, Firat University, Elazig 23119, Turkey; hfoztop1@gmail.com<sup>3</sup> Mechanical Engineering Department, Faculty of Engineering, King Abdulaziz University, P.O. Box 40844, Jeddah 21511, Saudi Arabia; nabuhamdeh@kau.edu.sa<sup>4</sup> Laboratory on Convective Heat and Mass Transfer, Tomsk State University, 634050 Tomsk, Russia

\* Correspondence: fatih.selimefendigil@cbu.edu.tr (F.S.); sheremet@math.tsu.ru (M.A.S.)

Received: 5 January 2019; Accepted: 15 January 2019; Published: 19 February 2019



**Abstract:** In this study, forced convection of Fe<sub>3</sub>O<sub>4</sub>-water nanofluid in a bifurcating channel was numerically studied under the influence of variable magnetic. Galerkin residual finite element method was used for numerical simulations. Effects of various values of Reynolds number (between 100 and 500), Hartmann number (between 0 and 3), and solid nanoparticle volume fraction (between 0% and 4%) on the convective heat transfer characteristics were analyzed. It was observed that location and size of the re-circulation zones established in the walls of the bifurcating channel strongly influenced by the variable magnetic field and Reynolds number. Average Nusselt number versus Hartmann number showed different characteristics for hot walls of the vertical and horizontal branching channels. The average Nusselt number enhancements were in the range of 12–15% and 9–12% for hot walls of the branching channel in the absence and presence of magnetic field (at Hartmann number of 3).

**Keywords:** variable magnetic field; MHD flow; finite element method; Fe<sub>3</sub>O<sub>4</sub>-water

## 1. Introduction

Effects of magnetic field are encountered in some engineering applications such as in geothermal energy extraction, nuclear reactor coolers, and metal casting. In convective heat transfer applications, an external magnetic field may be used to control the fluid flow and heat transfer characteristics. In many cavity flow applications with convection, magnetic field dampens the fluid motion and reduces the convective heat transfer rate [1,2]. In jet flow configurations, magnetic field effects reduce the unsteady effects. A potential application of magnetic field is to enhance the heat transfer for the configurations with separated flows such as encountered in a backward-facing step and branching channel. The size of the re-circulation zones can be altered with an externally imposed magnetic field in a convective heat transfer with separated flow. Magnetic field effects in convection can be altered by adding nano-sized particles to the base fluid, which changes both the thermal and electrical conductivity of the fluid [3,4]. The inclusion of a very small amount of nanoparticles to the base fluid may result in significant enhancement of heat transfer, and various factors affect the amount of enhancement, such as size, shape and type of the particles. Nanofluid technology has been successfully implemented in various thermal engineering application [5,6]. Mehryan et al. [7] examined the entropy generation study of Fe<sub>3</sub>O<sub>4</sub>-water nanofluid in an enclosure under the effect of variable magnetic field. A spatially sinusoidal varying magnetic field in y-direction was imposed and differences were noted when compared to a case with uniform magnetic field. Sheikholeslami and Ganji [8] analyzed ferrofluid

flow in a semi annulus with an external magnetic field by using control volume based finite element method (CVFEM) considering both ferrodynamics and magnetohydrodynamics. Magnetic number was found to influence the heat transfer differently depending on the Rayleigh number while both increasing nanoparticle volume fraction and decreasing Hartmann number were found to enhance the heat transfer rate. In the numerical study by Sheikholeslami et al. [9], forced convection of magnetic nanofluid in a lid-driven semi annulus was examined with CVFEM. The average Nusselt number was observed to increase with nanoparticle volume fraction while the heat transfer enhancement was found to decrease with higher values of Reynolds number and lower values of Hartmann number. Selimefendigil and Oztop [10] performed a numerical Magneto-hydrodynamic nanofluid convection of a vented cavity with elastic step-wise corrugation of the walls by using finite element method. The presence of the magnetic field was found to affect the distribution of multiple recirculation zones within the vented cavity filled with nanofluid. In a recent numerical study, efficiency of a direct absorption solar collector was examined with nanofluid and magnetic field effects. In the case of magnetic nanofluid, efficiencies up to 30% were obtained.

Flow separation is important in many engineering applications, e.g. in aerodynamics, power generation systems, thermal energy storage, and many others [11,12]. Fluid flow geometries are prone to such fluid phenomena as branching channels and backward or forward facing steps [13,14]. Fluid flow and heat transfer characteristics in branching channel are important in many applications ranging from biomedical to pharmaceutical industry. Matos and Oliveira [15] performed numerical simulation for fluid flow of non-Newtonian inelastic fluid in a bifurcating channel. Fluid flow characteristic were found to be influenced by the variation of Reynolds number, mass flow rate ratio and power-law index values. Senn and Poulikakos [16] performed numerical study for analyzing the effects of secondary flow on the thermal mixing in a tree-like micro-channel net. Selimefendigil and Oztop [17] numerically analyzed convection of nanofluid flow for a backward-facing step geometry with a uniform magnetic field, which was imposed at various inclination angles. It was observed that, for vertically and inclined application of magnetic field, re-circulation zone behind the step was reduced and heat transfer augmented for higher values of Hartmann number. In the study by Abbassi and Nassrallah [18], laminar flow of electrically conducting fluid in a backward-facing step geometry was analyzed. Various values of Stuart number and Prandtl number were considered for Reynolds number of 380. For higher values of Prandtl number, magnetic field was found to enhance the heat transfer, whereas, except in the regions of recirculation zone, fluid motion was dampened by the magnetic field. An experimental study of pulsating fluid flow in laminar conditions through a 90-degree bifurcation was performed by Khodadadi et al. [19]. They observed that the Reynolds number, dividing mass flow rate of the branching channels and Stokes number have influence on the formation and size of the re-circulation regions. A theoretical study for the forced convective heat transfer in a branch network was conducted by Luo et al. [20]. The heat transfer rate was found to increase with trunk diameter and deteriorate with the length of the branched structure. In a recent study, Selimefendigil et al. [21] performed numerical study of branching channel of CuO–water nanofluid under the effects of uniform magnetic field. The influences of inclination angle of lower branching channel and Hartmann number in uniform magnetic field on the convective heat transfer features were examined. The average Nusselt number was found to be higher for higher values of Hartmann number, while the addition of nanoparticle was found to be efficient for higher values of Hartmann number. Selimefendigil and Oztop [22] made a numerical study on the convective heat transfer features of a branching channel filled with carbon nanotube (CNT)-water nanofluid under the effects of rotating surface at the junction. Significant enhancement was observed with the inclusion of CNT nanoparticles to the base fluid, while the convective heat transfer features were found to be strongly influenced by the rotation of the surface at the junction.

This study focused on the convective heat transfer characteristics of  $\text{Fe}_3\text{O}_4$ –water nanofluid in a T-junction with a variable magnetic field where flow separation and reattachment exist. In this configuration, the magnetic field has the potential to reduce the separated flow region, the effect of electrical conductivity enhancement with nanoparticle inclusion to the base fluid is favorable, and the

increment in the heat transfer rate might be obtained. The originality of this study is that a non-uniform magnetic field was imposed and different heated walls of a bifurcating channel were examined with the presence of nanoparticles. The numerical results of this study can be utilized in the thermal design and optimization of fluid flow with separation and will be helpful in determining the conditions to impose a variable magnetic field and nanoparticles.

## 2. Numerical Modeling

A schematic view of the computational domain of bifurcating channel with a magnetic source is shown in Figure 1 with boundary conditions. A bifurcating T-channel with channel heights  $H_1=H_2=H_3=H$  and lengths  $S_1=S_2=S_3=50H$  was considered. The existing channels (horizontal and vertical) of the branching geometry were kept at constant temperature ( $T_h$ ) while the fluid entered at the inlet of the first channel with velocity  $u_0$  and temperature ( $T_c$ ) with  $T_h > T_c$ . A magnetic wire was placed below the horizontal wall vertically to the  $xy$ -plane with locations  $(c, d)$  with  $c = 4H$  and  $d = -4H$ . We considered  $Fe_3O_4$ -water nanofluid and assumed incompressible, Newtonian fluid. Thermophysical properties of water and  $Fe_3O_4$  nanoparticles are given in Table 1. The flow was two-dimensional, steady and laminar. Natural convection and radiation effects were neglected. Effects of induced magnetic field were neglected.

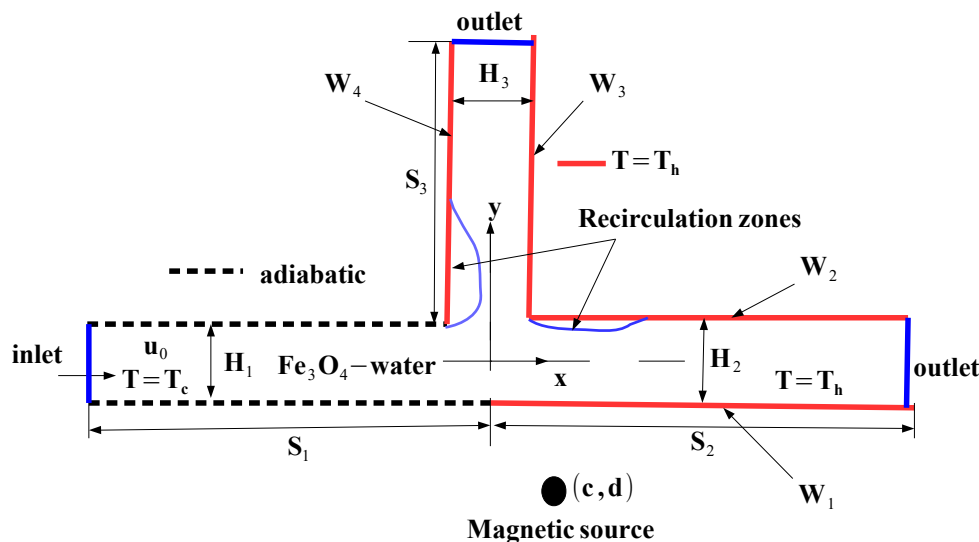


Figure 1. Schematic view of the physical model with boundary conditions.

Table 1. Thermophysical properties of water and  $Fe_3O_4$  nanoparticle.

Property	Water	$Fe_3O_4$
$\rho$ (kg/m <sup>3</sup> )	997.1	5200
$c_p$ (J/kg K)	4179	670
$k$ (W/mK)	0.61	6
$\mu$ (N s/m <sup>2</sup> )	0.001003	-
$\sigma$ ( $\Omega$ m) <sup>-1</sup>	0.05	25,000

Conservation equations for fluid flow and heat transfer are written as:

$$\frac{\partial u}{\partial x} + \frac{\partial v}{\partial y} = 0, \quad (1)$$

$$u \frac{\partial u}{\partial x} + v \frac{\partial u}{\partial y} = -\frac{1}{\rho_{nf}} \frac{\partial p}{\partial x} + \nu_{nf} \left( \frac{\partial^2 u}{\partial x^2} + \frac{\partial^2 u}{\partial y^2} \right) + F_x, \quad (2)$$

$$u \frac{\partial v}{\partial x} + v \frac{\partial v}{\partial y} = -\frac{1}{\rho_{nf}} \frac{\partial p}{\partial y} + \nu_{nf} \left( \frac{\partial^2 v}{\partial x^2} + \frac{\partial^2 v}{\partial y^2} \right) + F_y, \quad (3)$$

$$u \frac{\partial T}{\partial x} + v \frac{\partial T}{\partial y} = \alpha_{nf} \left( \frac{\partial^2 T}{\partial x^2} + \frac{\partial^2 T}{\partial y^2} \right) + \sigma_{nf} (uB_y - vB_x)^2 + \mu_{nf} \left( 2 \left( \frac{\partial u}{\partial x} \right)^2 + 2 \left( \frac{\partial v}{\partial x} \right)^2 + \left( \frac{\partial u}{\partial x} + \frac{\partial v}{\partial y} \right)^2 \right), \quad (4)$$

The Lorentz forces per unit volume in the MHD flow can be stated as:

$$F_x = -\sigma_{nf} B_y^2 u + \sigma_{nf} B_x B_y v, \quad F_y = \sigma_{nf} B_x B_y u - \sigma_{nf} B_x^2 v \quad (5)$$

with magnetic field intensity  $(H_x, H_y)$  for a magnetic source located at  $(c, d)$ :

$$H_x = \frac{\gamma}{2\pi} \frac{y-d}{(x-c)^2 + (y-d)^2}, \quad H_y = -\frac{\gamma}{2\pi} \frac{x-c}{(x-c)^2 + (y-d)^2} \quad (6)$$

Magnetic induction components are given by the

$$B_x = \mu_0 H_x, \quad B_y = \mu_0 H_y \quad (7)$$

The second term of the right hand side expression of the energy equation represents the Joule heating. Nanofluid density and heat capacity are defined by using:

$$\rho_{nf} = (1-\phi)\rho_f + \phi\rho_p, \quad (\rho c_p)_{nf} = (1-\phi)(\rho c_p)_f + \phi(\rho c_p)_p \quad (8)$$

The viscosity model of the nanofluid is described as:

$$\mu_{nf} = \frac{\mu}{(1-\phi)^{2.5}} \quad (9)$$

Thermal conductivity (Maxwell–Garnett model) and electrical conductivity (Maxwell model) of nanofluid are described as:

$$k_{nf} = k_f \left[ \frac{(k_p + 2k_f) - 2\phi(k_f - k_p)}{(k_p + 2k_f) + \phi(k_f - k_p)} \right], \quad \sigma_{nf} = \sigma_f \left[ 1 + \frac{3 \left( \frac{\sigma_p}{\sigma_f} - 1 \right) \phi}{\left( \frac{\sigma_p}{\sigma_f} + 2 \right) - \left( \frac{\sigma_p}{\sigma_f} - 1 \right) \phi} \right] \quad (10)$$

The non-dimensional form of the governing equations can be obtained by using the following dimensionless parameters:

$$\begin{aligned} U &= \frac{u}{u_0}, \quad V = \frac{v}{u_0}, \quad \theta = \frac{T - T_c}{T_h - T_c}, \quad X = \frac{x}{H}, \quad Y = \frac{y}{H}, \quad C = \frac{c}{H}, \\ D &= \frac{d}{H}, \quad P = \frac{p}{\rho_f u_0^2}, \quad (H_x, H_y) = \frac{(H_x, H_y)}{H_0}, \quad H_0 = \frac{\gamma}{2\pi|b|}, \\ Re &= \frac{u_0 H}{\nu_f}, \quad Pr = \frac{\nu_f}{\alpha_f}, \quad Ha = H \mu_0 H_0 \sqrt{\frac{\sigma_f}{m u_f}}, \quad Ec = \frac{u_0^2}{c_p \Delta T} \end{aligned} \quad (11)$$

Boundary conditions are stated as:

- At the inlet, temperature and velocity are uniform (parabolic with average value of  $u_0$ ),  $u = u_0, v = 0, T = T_c$ .
- Isothermal with no-slip boundary condition for the exist channel walls,  $u = v = 0, T = T_h$ .
- Outflow boundary conditions for the outlets,  $\frac{\partial u}{\partial x} = 0, v = 0, \frac{\partial T}{\partial x} = 0$ .

- Adiabatic wall, no-slip boundary boundary condition for other walls,  
 $u = v = 0, \frac{\partial T}{\partial n} = 0$ .

Local and average Nusselt number for the hot channel walls are evaluated as:

$$\text{Nu}_s = -\frac{k_{nf}}{k_f} \frac{\partial \theta}{\partial n}, \quad \text{Nu}_{m,i} = \frac{1}{L_i} \int_0^{L_i} \text{Nu}_s ds, \quad \text{Nu}_m = \frac{\sum_{i=1}^4 \text{Nu}_{m,i}}{4} \quad (12)$$

### 3. Solution, Mesh Independence and Code Validation Studies

Galerkin weighted residual finite element method was used for the solution of governing equations with boundary conditions. In this formulation, the weak form of the governing equations is established. When the flow variables (approximated variables) are inserted into the governing equations, residual  $R$  will be obtained. Weighted average of  $R$  is set to be zero as:

$$\int_{\Omega} WR dv = 0 \quad (13)$$

with  $W$  denoting the weight function. It was chosen from the same set of functions as the trial functions. Finally, nonlinear residual equations were achieved, which were solved using the Newton–Raphson method. Convergence of the solution was achieved when the relative error for each of the variables became less than  $10^{-5}$ . Grid independence test of the numerical solution was verified by using different number of grids. Grids were refined near the walls and in the junction of the branching channel to resolve higher gradients of the field variables. Table 2 presents average Nusselt numbers considering various grid sizes at different values of  $\phi$  and Ha values. G4 with 48,806 elements (rectangular and triangular) was chosen for the subsequent computations.

**Table 2.** Grid independence study for various grid sizes: Average Nusselt number for the hot walls of the branching channel for various combinations of Hartmann number and solid particle volume fraction ( $\text{Re} = 500$ ).

Ha	$\phi$	G1-735	G2-3380	NG3-7441	G4-48806	G5-90375
0	0	4.793	3.991	4.010	3.991	3.849
0	0.02	5.049	4.243	4.282	4.263	4.115
0	0.04	5.318	4.509	4.568	4.549	4.395
1	0	7.813	5.636	4.531	4.506	4.322
1	0.02	8.155	5.933	4.819	4.793	4.596
1	0.04	8.511	6.244	5.122	5.095	4.886
3	0	9.058	8.492	6.315	6.265	6.130
3	0.02	9.434	8.859	6.640	6.589	6.445
3	0.04	9.824	9.239	6.979	6.927	6.774

Numerical code was verified with with available data in the literature. The first validation study was made using the numerical results of Khandelwal et al. [23] for non-Newtonian fluid flow of right-angled T-channel. Table 3 shows a comparison of the recirculation lengths calculated at two different Reynolds number. In the second validation study, magnetic field effects were considered. Table 4 shows the comparison of average Nusselt number for various Hartmann numbers in Reference [24]. Numerical results of Sheikholeslami and Shamlooei [25] were also added where the simulation was performed with lattice Boltzmann method. From the comparison of the results, sufficient confidence in the accuracy of the current code was established.

**Table 3.** Code validation: Recirculation lengths in a right-angled T-channel.

Re	$L_R/D$ (Reference [23])	$L_R/D$ (Present)	Difference (%)
25	1.44	1.38	−4.17
200	3.99	3.96	−0.75

**Table 4.** Average Nusselt number comparisons for different Hartmann numbers for natural convection in a cavity under the effect of magnetic field.

Ha	Current Study	Sheikholeslami and Shamlooei [25]	Rudraiah et al. [24]
$Gr = 2 \times 10^4$			
0	2.474	2.566	2.518
10	2.172	2.266	2.223
100	1.009	1.022	1.011
$Gr = 2 \times 10^5$			
0	4.972	5.093	4.919
10	4.773	4.904	4.805
100	1.389	1.460	1.431

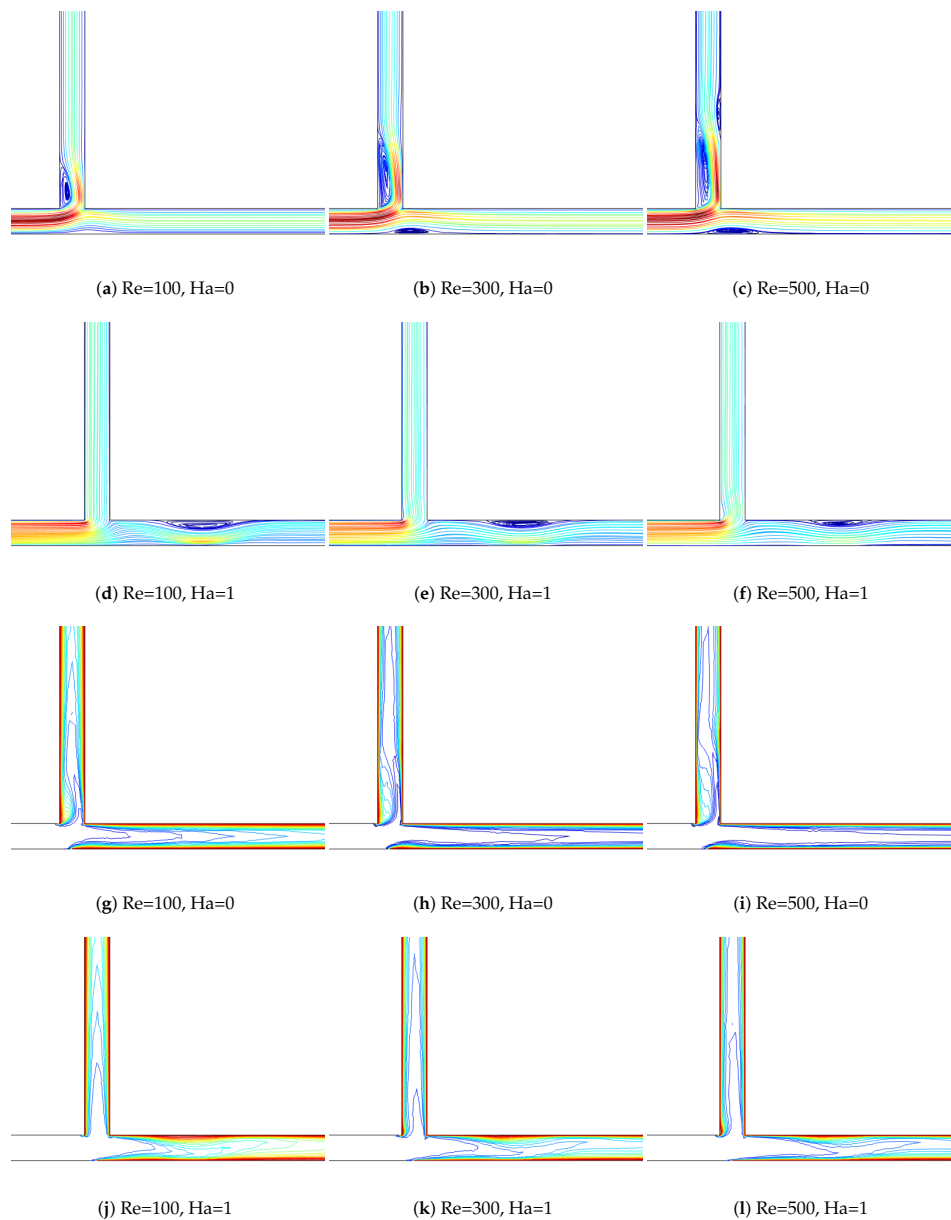
#### 4. Results and Discussion

In this study, forced convection of  $Fe_3O_4$ -water nanofluid flow in a branching T-channel was numerically examined with variable magnetic field effects. Numerical simulations were performed for various values of Reynolds number based on channel height (between 100 and 500), Hartmann number (between 0 and 3), and solid nanoparticle volume fraction (between 0% and 4%). The influence of those pertinent parameters on the convective heat transfer characteristics was analyzed. A particular attention was given to the effects of variable magnetic field on the flow separation at the junction of the branching channels.

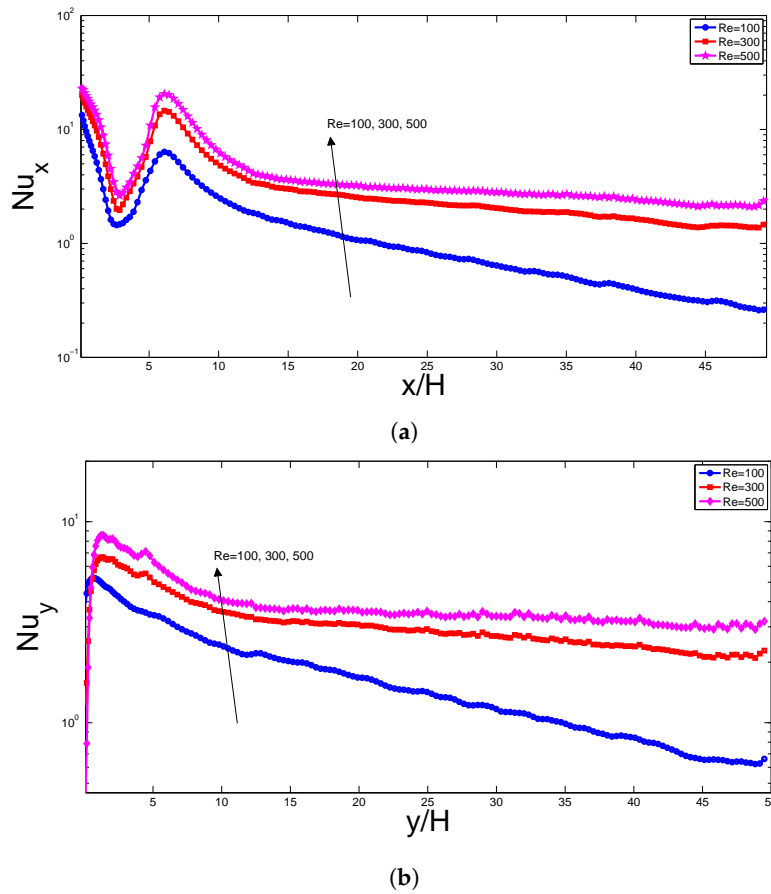
Effects of Reynolds number on the flow and thermal pattern distributions for the branching T-channel are demonstrated in Figure 2 ( $Ha = 1$ ,  $\phi = 0.02$ ). At low Reynolds number, a re-circulation vortex was established in the top wall of the upper branching channel. At Reynolds number of 300, this vortex extended in size and a small vortex was also seen in the bottom wall of the branching channel near the junction. Further increment of the Reynolds number to 500 resulted in an additional vortex appearing on the bottom wall of the upper branching channel. The location and size of the re-circulation zones for the exist channels were strongly influenced by the variation of Reynolds number. Thermal gradients became steeper along the walls with higher Reynolds number and distributions of the isotherms were influenced by the formation of the vortices for different Reynolds numbers. Figure 3 and Figure 4 show the local and average heat transfer enhancements for the hot wall of the exit channels with Reynolds number. The top wall of the horizontal exist channel and the top wall of vertical exist channel are shown as W2 and W4 in the figures. Variation of average Nusselt number for each of the hot wall of the T-junction considering various combinations of Reynolds number and solid particle volume fraction are shown in Table 5 ( $Ha = 1$ ). For walls W1 and W3, average Nusselt number enhancements were 10.4% and 11.3% for Reynolds number of 100, respectively whereas they became 12.2% and 14.1% for Reynolds number of 500 when highest solid volume fraction of nanoparticle was added to the base fluid.

Figure 5 shows the influence of Hartmann number on streamline and isotherm distributions for the branching channel with  $Re = 300$  and  $\phi = 0.02$ . In the previous studies where convection in cavity was considered, magnetic field was found to dampen the fluid motion and reduce the convection. In separated flow configuration, the re-circulation zones were rearranged and separation could be reduced, which has the potential to enhance the heat transfer rate. In the absence of magnetic field, two vortices were formed: one on the top wall of the vertical channel and the other one on the bottom wall of the horizontal exist channel near the junction. When magnetic field was imposed for  $Ha = 0.5$ , only the vortex on the top wall of the vertical channel appeared but its size was significantly reduced as compared to the case in the absence of magnetic field. Further increment of the Hartmann number to  $Ha = 3$  resulted in the establishment of the vortex on the top wall of the horizontal exit channel. The size and location of separated zones in the branching channels were strongly influenced by the variation of magnetic field. The clustering of the isotherms was denser in the location near the reattachment points and variation of temperature gradients along the hot wall of the branching channel was observed

when changing the strength of the magnetic field. Local variation of the Nusselt for the W2 and W4 walls are illustrated in Figure 6 for various values of Hartmann numbers. Peak values of the local Nusselt number and their locations were highly affected by the magnetic field, which was significant for the upper wall of the horizontal channel (W2). For wall W2, at location  $x = 7 H$ , a peak value of the Nusselt number was seen and it achieved the highest value at  $Ha = 3$ . This was attributed to the formation of the vortex and change of the reattachment length for this location with magnetic field. Except for some local locations, the magnetic field acted in a way to reduce the local Nusselt number.



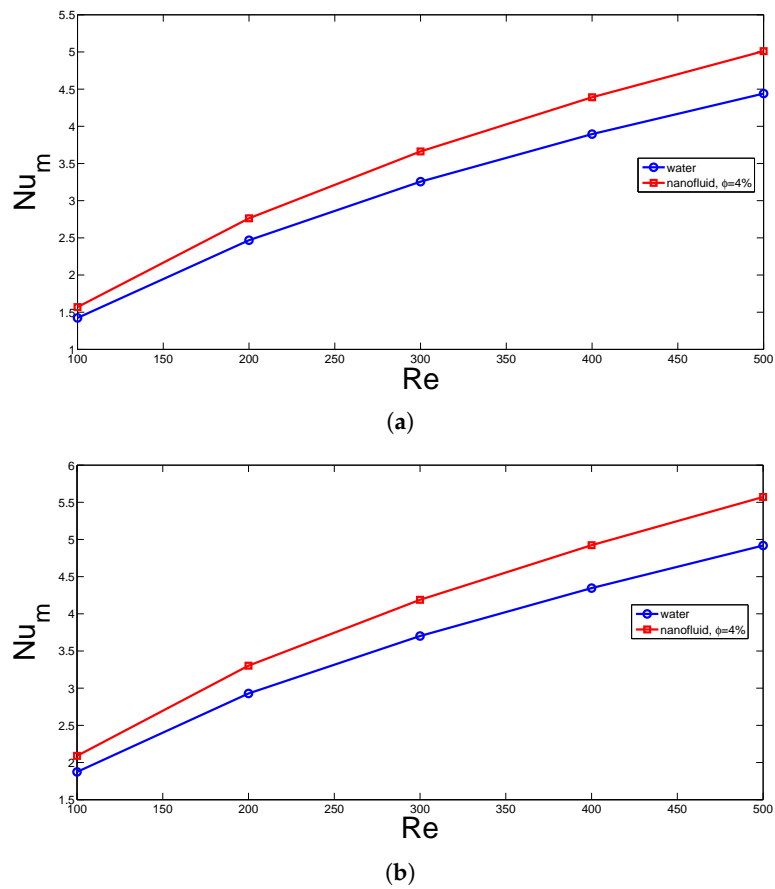
**Figure 2.** Effects of Reynolds number on the streamline (a–f) and isotherm (g–l) variations in the absence and presence of magnetic field ( $\phi = 0.02$ ).



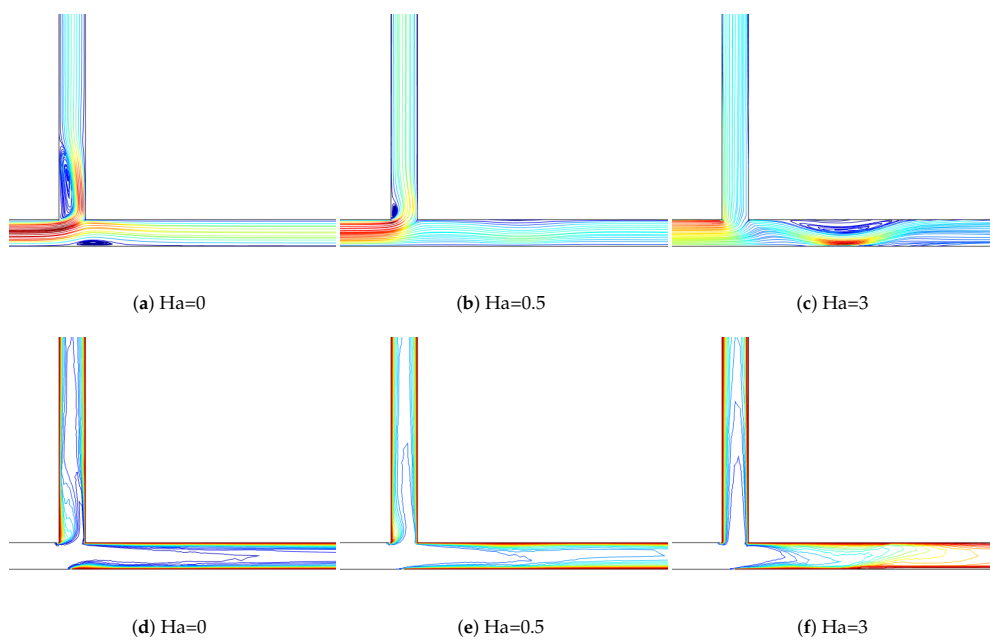
**Figure 3.** Variation of the local Nusselt number for the upper walls of the horizontal and vertical channels with respect to change in Reynolds number ( $Ha = 1, \phi = 0.02$ ): (a) W2, local Nusselt number variation; and (b) W4, local Nusselt number variation.

**Table 5.** Effects of Reynolds number and solid particle volume fraction combination on the variation of average Nusselt number for hot walls of the branching channel ( $Ha = 0$ ).

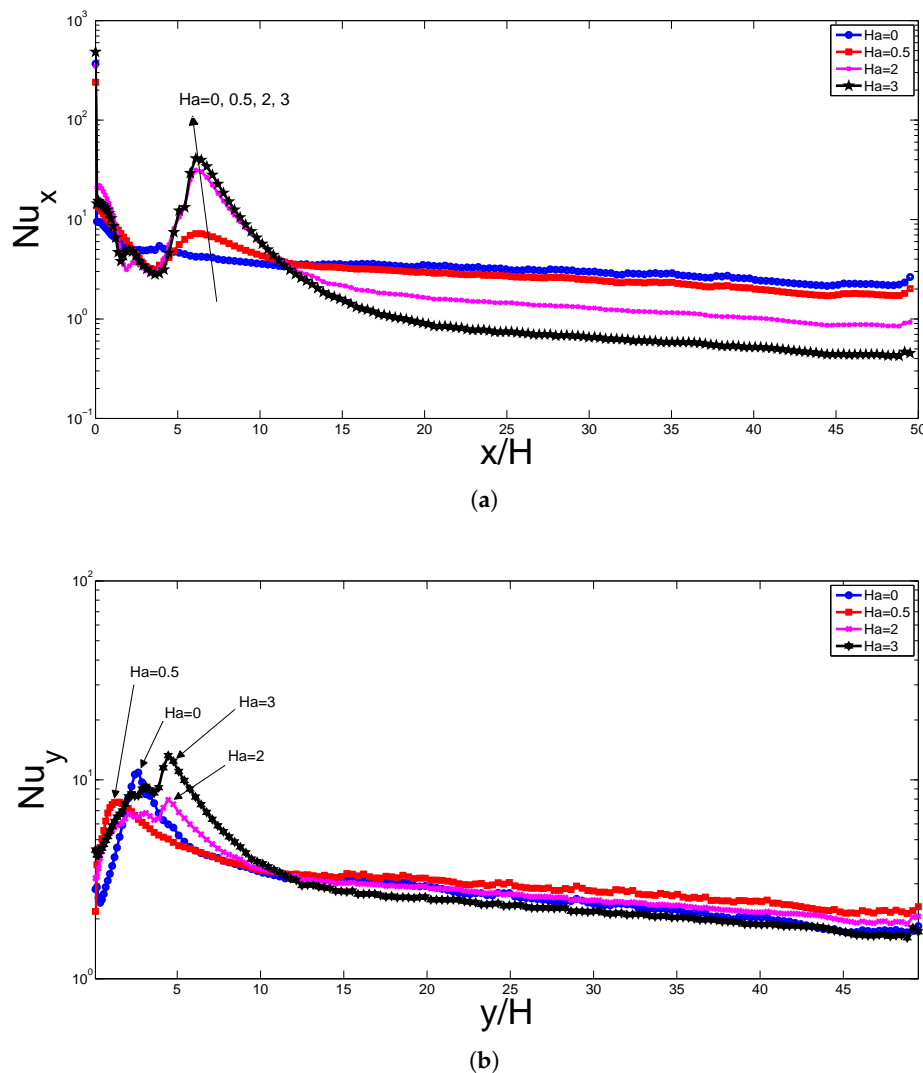
Re	$\phi$	$Nu_m$ (W1)	$Nu_m$ (W2)	$Nu_m$ (W3)	$Nu_m$ (W4)
100	0	1.507	1.423	1.701	1.873
100	0.01	1.545	1.458	1.748	1.926
100	0.02	1.584	1.495	1.796	1.979
100	0.03	1.624	1.532	1.844	2.034
100	0.04	1.664	1.569	1.894	2.089
200	0	2.531	2.468	2.592	2.928
200	0.01	2.602	2.539	2.672	3.018
200	0.02	2.675	2.613	2.756	3.111
200	0.03	2.750	2.687	2.840	3.205
200	0.04	2.826	2.762	2.927	3.302
300	0	3.313	3.255	3.198	3.701
300	0.01	3.409	3.353	3.302	3.818
300	0.02	3.509	3.454	3.410	3.939
300	0.03	3.610	3.557	3.520	4.062
300	0.04	3.713	3.661	3.633	4.188
400	0	3.977	3.894	3.680	4.345
400	0.01	4.093	4.014	3.803	4.484
400	0.02	4.213	4.137	3.930	4.627
400	0.03	4.335	4.262	4.060	4.773
400	0.04	4.461	4.390	4.193	4.923
500	0	4.567	4.440	4.097	4.918
500	0.01	4.701	4.577	4.235	5.075
500	0.02	4.838	4.718	4.378	5.236
500	0.03	4.979	4.863	4.52	5.402
500	0.04	5.123	5.010	4.674	5.571



**Figure 4.** Effects of Reynolds number on the variation of the average Nusselt number for the upper walls of the horizontal and vertical channels with respect to change in Reynolds number ( $Ha = 1$ ): (a) W2, average Nusselt number variation; and (b) W4, average Nusselt number variation.



**Figure 5.** Streamline (a–c); and isotherm (d–f) distribution for various values of Hartmann numbers ( $Re = 300, \phi = 0.02$ ).



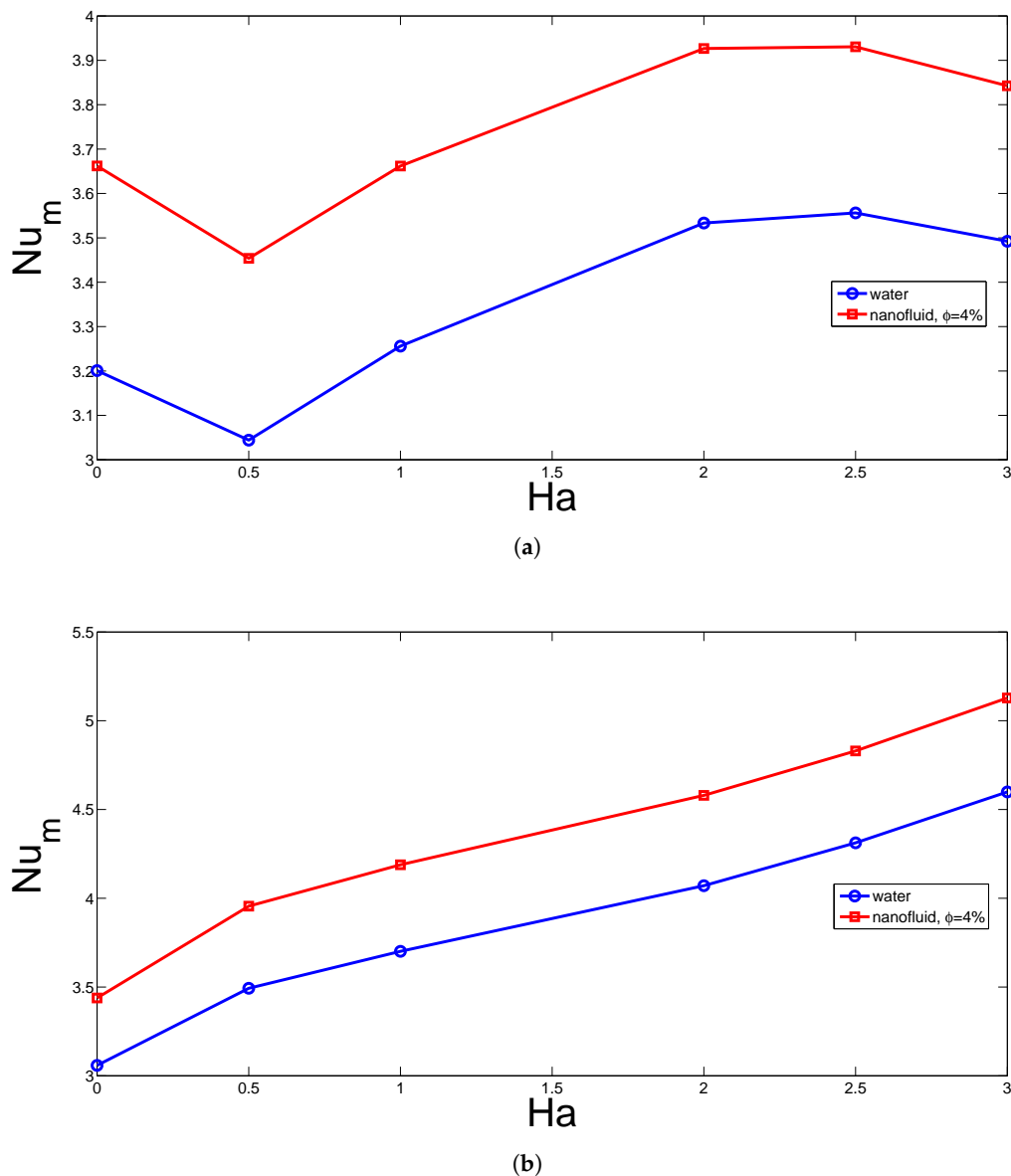
**Figure 6.** Effects of Hartmann number on the local Nusselt number variations for the upper hot walls of the vertical and horizontal exit channels ( $Re = 300$ ,  $\phi = 0.02$ ): (a) W2, local Nusselt number variation; and (b) W4, local Nusselt number variation.

Figure 7 shows the variation of the average Nusselt number with respect to changes in the Hartmann number for walls W2 and W4 for water and nanofluid ( $\phi = 4\%$ ). For wall W4, magnetic field results in heat transfer enhancement both for fluid and nanofluid. Maximum enhancements were 50.3% and 49.2% for water and nanofluid (from  $Ha = 0$  to  $Ha = 3$ ), respectively. Enhancement of heat transfer rate for the upper wall of the vertical channel (W4) was attributed to the favorable effect of magnetic field strength on the suppression of the re-circulation zone for wall W4. On the other hand, for wall W2, magnetic field first deteriorated the average heat transfer rate from  $Ha = 0$  to  $Ha = 0.5$ , then increased until  $Ha = 2$  and finally deteriorated thereafter. The maximum and minimum average Nusselt number values were achieved in the presence of magnetic field for  $Ha = 0.5$  and  $Ha = 2$  (for wall W2), respectively. The average Nusselt number variations for other walls of the existing channels of the T-junction are given in Table 6 for different values of Hartmann number and solid particle volume fraction. The trends in the variation were similar for walls W1-W2 and for walls W3-W4. In the absence and presence of magnetic field, adding nanoparticles to the base fluid had different effects on heat transfer enhancements. This was attributed to the competing effects such as favorable effect of electrical conductivity enhancement with nanoparticle inclusion in the

presence of magnetic field for separated flow, thermal conductivity enhancement and increase of the viscosity with nanoparticle inclusion to the base fluid. In the absence of magnetic field ( $Ha = 0$ ), enhancements in the average heat transfer rates with nanoparticle inclusion were 14.5% and 12.4% for walls W2 and W4, respectively, while in the presence of magnetic field ( $Ha = 3$ ), these values were reduced to 10% and 11.5%. The influence of variable magnetic field strength changed the heat transfer enhancement characteristics differently for walls W2 and W4 with nanoparticle inclusion to the base fluid. The amount of reduction was higher for wall W2 compared to wall W4. As the magnetic field strength changed, the fluid motion dampened but the separation zone was redistributed. Near the upper channel of horizontal wall (W2), an additional vortex appeared at the highest value of Hartmann number while the vortex established at  $Ha = 0$  in the vicinity of the upper channel of vertical wall disappeared (Figure 5). The interaction of various effects, such as dampening of fluid motion with magnetic field and suppression of recirculation zones with magnetic field, resulted in less reduction of the average Nusselt number for wall W4 as compared to wall W2 in terms of heat transfer enhancement with nanoparticle inclusion to the base fluid when magnetic field was imposed. In a recent study, Selimefendigil et al. [21] examined the influence of inclination angle of lower branching channel in a bifurcating channel with uniform magnetic field. The uniform magnetic field in the channel was found to suppress the recirculation zones and resulted in the average Nusselt number enhancement. The important finding in the current study is that the characteristics of heat transfer enhancement with MHD nanofluid is different when uniform and non-uniform magnetic fields are imposed in a branching channel where multiple flow separations and reattachments occur.

**Table 6.** Effects of Hartmann number and solid particle volume fraction combination on the variation of average Nusselt number for hot walls of the branching channel ( $Re = 300$ ).

Ha	$\phi$	$Nu_m$ (W1)	$Nu_m$ (W2)	$Nu_m$ (W3)	$Nu_m$ (W4)
0	0	3.0634	3.2009	2.9285	3.0585
0	0.01	3.1701	3.3117	3.02	3.1498
0	0.02	3.2803	3.4259	3.1144	3.2439
0	0.03	3.3929	3.5427	3.2109	3.3401
0	0.04	3.5079	3.6621	3.3095	3.4382
0.5	0	2.9885	3.0442	3.0887	3.493
0.5	0.01	3.0842	3.1428	3.192	3.6043
0.5	0.02	3.1826	3.2442	3.2985	3.7188
0.5	0.03	3.2834	3.348	3.4076	3.836
0.5	0.04	3.3863	3.4539	3.5191	3.9557
1	0	3.3134	3.256	3.1981	3.7012
1	0.01	3.4099	3.354	3.3025	3.8184
1	0.02	3.5095	3.4549	3.4104	3.9397
1	0.03	3.6106	3.5574	3.5207	4.0629
1	0.04	3.7136	3.6619	3.6334	4.1888
2	0	4.1255	3.5334	3.5697	4.0708
2	0.01	4.2294	3.6292	3.677	4.1929
2	0.02	4.3359	3.727	3.7877	4.3187
2	0.03	4.4444	3.8264	3.9013	4.448
2	0.04	4.5545	3.9267	4.0174	4.5794
2.5	0	4.5627	3.5561	3.7994	4.312
2.5	0.01	4.6706	3.6475	3.9092	4.4364
2.5	0.02	4.7812	3.7409	4.0231	4.5652
2.5	0.03	4.8935	3.8352	4.1392	4.6961
2.5	0.04	5.0075	3.9305	4.2582	4.83
3	0	4.988	3.4924	4.0213	4.5991
3	0.01	5.1002	3.5782	4.1346	4.7265
3	0.02	5.2153	3.6656	4.2518	4.8579
3	0.03	5.3324	3.7537	4.3714	4.9918
3	0.04	5.4514	3.8427	4.4936	5.1284



**Figure 7.** Average Nusselt number versus Hartmann number variations for the upper hot walls of the vertical and horizontal exit channels for water and nanofluid ( $Re = 300$ ): (a) W2, average Nusselt number variation; and (b) W4, average Nusselt number variation.

A polynomial relation for the average Nusselt number with respect to changes in Reynolds number and Hartmann number were obtained for water and nanofluid with  $\phi = 4\%$ . It was second-order in terms of Reynolds number and Hartmann number, which is defined as:

$$Nu(Re', Ha') = p00 + p10 * Re' + p01 * Ha' + p20 * Re'^2 + p11 * Re' * Ha' + p02 * Ha'^2 \quad (14)$$

where  $Re' = \frac{Re-300}{143.8}$  and  $Ha' = \frac{Ha-1.5}{1.099}$  are the modified Reynolds number and Hartmann numbers. The coefficients of the polynomial fit are given in Table 7 for water and nanofluid model within their %95 confidence interval. Table 8 presents the results of R-square and root mean square values (RMSE) for each of the models. Figure 8a,b shows the approximated surface with polynomial fit with CFD data and residuals for water.

**Table 7.** Polynomial fit coefficients for water and nanofluid model (within their 95% confidence interval).

Coefficients	M1 (Water)	M2 (Nanofluid)
p00	3.581 (3.535, 3.626)	4.019 (3.971, 4.066)
p10	2.168 (2.102, 2.233)	1.349 (1.326, 1.372)
p01	0.4672 (0.4452, 0.4892)	0.4826 (0.4597, 0.5055)
p20	−0.1508 (−0.1775, −0.1241)	−0.1741 (−0.2019, −0.1463)
p11	0.2895 (0.2671, 0.3118)	0.3053 (0.282, 0.3286)
p02	0.05073 (0.01912, 0.08233)	0.05007 (0.01714, 0.08301)

**Table 8.** Root mean square (RMSE) and correlation coefficient (R-square) values for water and nanofluid model.

Modal Coeffs	R-square	RMSE
M1 (water)	0.9984	0.05734
M2 (nanofluid)	0.9986	0.05975

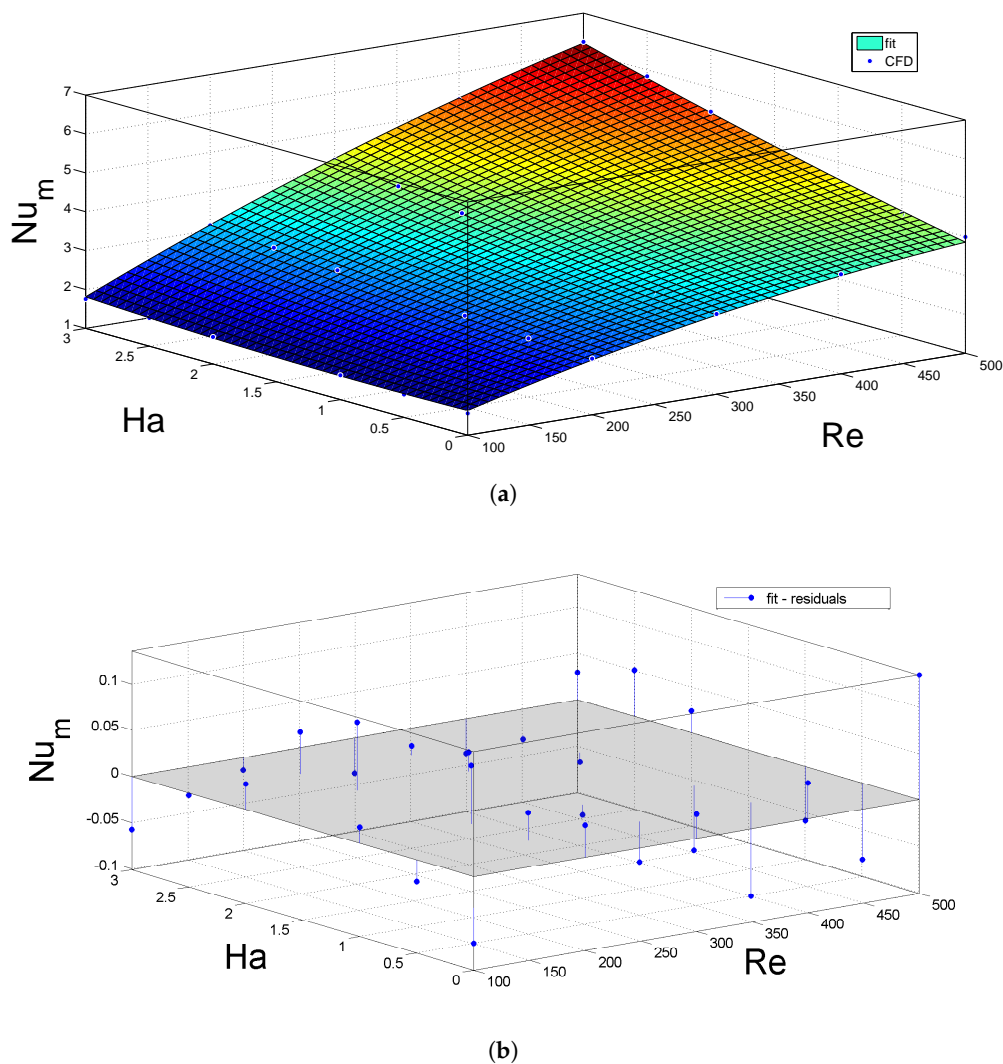


**Figure 8.** Surface fit with polynomials (average Nusselt number for the hot walls) and residuals with respect to changes in Reynolds and Hartmann number: (a) polynomial fit to the CFD data; and (b) residuals between the polynomial fit and CFD data.

## 5. Conclusions

Numerical simulation of forced convection for Fe<sub>3</sub>O<sub>4</sub>–water nanofluid in a bifurcating channel in the presence of variable magnetic field was numerically analyzed. The potential of magnetic field effects to reshape the separated region and to increase the local and average heat transfer was examined in a branching channel. It was observed that significant changes in the location and size of the re-circulation zones established in the walls of the existing channels of the bifurcating channel. This in turn resulted in the formation of local Nusselt number peaks and changed their locations on the hot walls. Variation of average Nusselt number showed different average heat transfer behavior with respect to changes in Hartmann number for walls of the vertical and horizontal branching channels. The average enhancements in the heat transfer rate was in the range of 12–15% for hot walls of the branching channel in the absence of magnetic field, whereas they were reduced by 9–12% in the presence of magnetic field at Hartmann number of 3. The present study can be extended to include the effects of various nanoparticle types, shape effects of nanoparticles, location of magnetic dipole source, aspect ratio of the channels and natural convection effects, which would enrich the applicability of the numerical findings for various applications of bifurcating channels encountered in practice.

**Author Contributions:** F.S. performed the numerical simulations and wrote some sections of the manuscript. Other authors prepared some other sections of the paper and analyzed the results. All of the authors contributed equally for reviewing and revising the manuscript.

**Funding:** This research received no external funding.

**Conflicts of Interest:** The authors declare no conflict of interest.

## Abbreviations/Nomenclature

$B$	magnetic induction
$c, d$	location of magnetic source, (m)
$H$	channel height, (m)
$Ha$	Hartmann number
$k$	thermal conductivity, ( $W\ m^{-1}\ K^{-1}$ )
$n$	unit normal vector
$Nu_x$	local Nusselt number
$Nu_m$	average Nusselt number
$p$	pressure, (Pa)
$Pr$	Prandtl number
$Re$	Reynolds number
$S$	channel length, (m)
$T$	temperature, (K)
$u, v$	x-y velocity components, ( $m\ s^{-1}$ )
$x, y$	Cartesian coordinates, (m)

### Greek Characters

$\alpha$	thermal diffusivity, ( $m^2\ s^{-1}$ )
$\sigma$	electrical conductivity, ( $S\ m^{-1}$ )
$\phi$	solid volume fraction
$\nu$	kinematic viscosity, ( $m^2\ s^{-1}$ )
$\theta$	non-dimensional temperature
$\rho$	density of the fluid, ( $kg\ m^{-3}$ )

### Subscripts

$c$	cold
$h$	hot
$m$	average
$nf$	nanofluid
$p$	solid particle

## References

1. Selimefendigil, F.; Chamkha, A.J. Magnetohydrodynamics Mixed Convection in a Lid-Driven Cavity Having a Corrugated Bottom Wall and Filled with a Non-Newtonian Power-Law Fluid Under the Influence of an Inclined Magnetic Field. *J. Therm. Sci. Eng. Appl.* **2016**, *8*, 021023. [[CrossRef](#)]
2. Sarris, I.; Zikos, G.; Grecos, A.; Vlachos, N. On the limits of validity of the low magnetic Reynolds number approximation in MHD natural-convection heat transfer. *Numer. Heat Transf. Part B* **2006**, *50*, 158–180. [[CrossRef](#)]
3. Selimefendigil, F.; Oztop, H.F. Numerical study of MHD mixed convection in a nanofluid filled lid driven square enclosure with a rotating cylinder. *Int. J. Heat Mass Transf.* **2014**, *78*, 741–754. [[CrossRef](#)]
4. Sheikholeslami, M.; Bandpy, M.G.; Ellahi, R.; Zeeshan, A. Simulation of MHD CuO-water nanofluid flow and convective heat transfer considering Lorentz forces. *J. Magn. Magn. Mater.* **2014**, *369*, 69–80. [[CrossRef](#)]
5. Mahian, O.; Kianifar, A.; Heris, S.Z.; Wen, D.; Sahin, A.Z.; Wongwises, S. Nanofluids effects on the evaporation rate in a solar still equipped with a heat exchanger. *Nano Energy* **2017**, *36*, 134–155. [[CrossRef](#)]
6. Yang, Y.T.; Lai, F.H. Numerical study of heat transfer enhancement with the use of nanofluids in radial flow cooling system. *Int. J. Heat Mass Transf.* **2010**, *53*, 5895–5904. [[CrossRef](#)]
7. Mehryan, S.A.M.; Izadi, M.; Chamkha, A.J.; Sheremet, M.A. Natural convection and entropy generation of a ferrofluid in a square enclosure under the effect of a horizontal periodic magnetic field. *J. Mol. Liq.* **2018**, *263*, 510–525. [[CrossRef](#)]
8. Sheikholeslami, M.; Ganji, D.D. Ferrohydrodynamic and magnetohydrodynamic effects on ferrofluid flow and convective heat transfer. *Energy* **2014**, *75*, 400–410. [[CrossRef](#)]
9. Sheikholeslami, M.; Rashidi, M.M.; Ganji, D.D. Effect of non-uniform magnetic field on forced convection heat transfer of Fe<sub>3</sub>O<sub>4</sub>-water nanofluid. *Comput. Methods Appl. Mech. Eng.* **2015**, *294*, 299–312. [[CrossRef](#)]
10. Selimefendigil, F.; Oztop, H.F. Fluid-solid interaction of elastic-step type corrugation effects on the mixed convection of nanofluid in a vented cavity with magnetic field. *Int. J. Mech. Sci.* **2019**, *152*, 185–197. [[CrossRef](#)]
11. Abu-Mulaweh, H. A review of research on laminar mixed convection flow over backward- and forward facing steps. *Int. J. Therm. Sci.* **2003**, *42*, 897–909. [[CrossRef](#)]
12. Selimefendigil, F.; Oztop, H.F. Effect of a rotating cylinder in forced convection of ferrofluid over a backward facing step. *Int. J. Heat Mass Transf.* **2014**, *71*, 142–148. [[CrossRef](#)]
13. Barkley, D.; Gabriela, M.; Gomes, M.; Henderson, R.D. Three-dimensional instability in flow over a backward-facing step. *J. Fluid Mech.* **2002**, *473*, 167–190. [[CrossRef](#)]
14. Selimefendigil, F.; Oztop, H.F. Control of Laminar Pulsating Flow and Heat Transfer in Backward-Facing Step by Using a Square Obstacle. *J. Heat Transf.* **2014**, *136*, 081701. [[CrossRef](#)]
15. Matos, H.; Oliveira, P. Steady and unsteady non-Newtonian inelastic flows in a planar T-junction. *Int. J. Heat Fluid Flow* **2013**, *39*, 102–126. [[CrossRef](#)]
16. Senn, S.; Poulikakos, D. Laminar mixing, heat transfer and pressure drop in tree-like microchannel nets and their application for thermal management in polymer electrolyte fuel cells. *J. Power Sour.* **2004**, *130*, 178–191. [[CrossRef](#)]
17. Selimefendigil, F.; Oztop, H.F. Influence of inclination angle of magnetic field on mixed convection of nanofluid flow over a backward facing step and entropy generation. *Adv. Powder Technol.* **2015**, *26*, 1663–1675. [[CrossRef](#)]
18. Abbassi, H.; Nassrallah, S.B. MHD flow and heat transfer in a backward-facing step. *Int. Commun. Heat Mass Transf.* **2007**, *34*, 231–237. [[CrossRef](#)]
19. Khodadadi, J.M.; Vlachos, N.S.; Liepsch, D.; Moravec, S. LDA Measurements and Numerical Prediction of Pulsatile Laminar Flow in a Plane 90-Degree Bifurcation. *J. Biomech. Eng.* **1988**, *110*, 129–136. [[CrossRef](#)] [[PubMed](#)]
20. Luo, L.; Tian, F.; Cai, J.; Hu, X. The convective heat transfer of branched structure. *Int. J. Heat Mass Transf.* **2018**, *116*, 813–816. [[CrossRef](#)]
21. Selimefendigil, F.; Oztop, H.F.; Chamkha, A.J. Role of magnetic field on forced convection of nanofluid in a branching channel. *Int. J. Numer. Methods Heat Fluid Flow* **2019**, in press. [[CrossRef](#)]

22. Selimefendigil, F.; Oztop, H.F. Numerical analysis and ANFIS modeling for mixed convection of CNT-water nanofluid filled branching channel with an annulus and a rotating inner surface at the junction. *Int. J. Heat Mass Transf.* **2018**, *127*, 583–599. [[CrossRef](#)]
23. Khandelwal, V.; Dhiman, A.; Baranyi, L. Laminar flow of non-Newtonian shear-thinning fluids in a T-channel. *Comput. Fluids* **2015**, *108*, 79–91. [[CrossRef](#)]
24. Rudraiah, N.; Barron, R.; Venkatachalappa, M.; Subbaraya, C. Effect of a magnetic field on free convection in a rectangular enclosure. *Int. J. Eng. Sci.* **1995**, *33*, 1075–1084. [[CrossRef](#)]
25. Sheikholeslami, M.; Shamlooei, M. Convective flow of nanofluid inside a lid driven porous cavity using CVFEM. *Physica B* **2017**, *521*, 239–250. [[CrossRef](#)]



© 2019 by the authors. Licensee MDPI, Basel, Switzerland. This article is an open access article distributed under the terms and conditions of the Creative Commons Attribution (CC BY) license (<http://creativecommons.org/licenses/by/4.0/>).